DOI 10.24425/aee.2025.153912

# Relative permittivity and electric strength at AC and surge voltage of dielectrics printed by focused deposition modelling

SEBASTIAN HAJDER<sup>®</sup>, JAROSŁAW WIŚNIOWSKI<sup>®</sup>, KAMIL FILIK<sup>®⊠</sup>, RADOSŁAW DROŻDŻOWSKI

Faculty of Electrical and Computer Engineering, Rzeszow University of Technology Al. Powstańców Warszawy 12, 35-959 Rzeszów, Poland

 $e\text{-mail:} \boxtimes \{s. hajder/j. wisniowski/kfilik\} @prz.edu.pl, \ ridekdro @gmail.com$ 

(Received: 20.02.2025, revised: 14.08.2025)

**Abstract:** A study of the relative permittivity and electric strength of dielectrics printed by focus deposition modeling was presented. These electrical parameters determined the lifetime reliability of devices made of dielectrics. Samples of PLA, ABS, PETG and ASA were tested according to IEC specifications. The dependence of the electrical properties of the samples on the type of material and printing precision was observed. Relative permittivity tests were carried out in the acoustic frequency band from 20 Hz to 20 kHz. It allowed analysis in a higher band than has been done in other publications to date. The electric strength of materials at 1.2/50 μs surge voltage was examined, which has not been widely analyzed before. Weibull plots, as a basis for determining the risk of failure, were prepared. The PETG FR (flame retardant) had the highest electric strength value, while PLA had the lowest. The differences with respect to tests at AC voltage were demonstrated. The printing technique affects the electrical strength value and location of potential electrical breakdown.

**Key words:** 3D printing, dielectrics, electric strength, lightning surge, relative permittivity, voltage tests

## 1. Introduction

3D printing technology, is one of the most innovative methods of prototyping that has gained popularity in recent years. Fused deposition modeling (FDM) is one of the most widely used 3D printing methods. The technology involves the layering of molten material, which then solidifies into the desired shape [1,2].



© 2025. The Author(s). This is an open-access article distributed under the terms of the Creative Commons Attribution-NonCommercial-NoDerivatives License (CC BY-NC-ND 4.0, https://creativecommons.org/licenses/by-nc-nd/4.0/), which permits use, distribution, and reproduction in any medium, provided that the Article is properly cited, the use is non-commercial, and no modifications or adaptations are made.

Due to its dielectric properties, such printing can be used in the prototyping of electrical or electronic devices [3]. Many entities are realizing increasingly complex electronic circuits using 3D printing technology, where, instead of a classical laminate such as FR-4 with an applied copper layer etched at a later stage to obtain conductive paths between electronic components, a substrate of non-conductive plastic is used, and the conductive paths are made from a specially prepared conductive filament [4–6]. As the studies in the above publications show, manufacturing of electronic circuits using this technology not only speeds up the whole process, but also saves space, as it is possible to use multiple layers in close proximity to each other with electronic components applied to them. In addition, 3D printing technology allows for increased recycling of plastic waste. As demonstrated by the authors of the article [7], it is possible to produce printed circuit boards (PCBs) in the so-called eco-friendly process using waste as an additive to the filament, and the authors, who conducted tests, did not find any negative impact of the use of such admixtures on the final PCB obtained. 3D printing can also be used in the production of high-voltage equipment, such as insulating components [8]. However, research in this area is not yet sufficiently developed. The authors of this publication emphasize that while they obtained promising results in terms of the dielectric properties of the printed material, the mechanical properties were inferior compared to classical methods of component fabrication such as injection molding, which still requires refinement of the printing technology.

With a view to the potential use of 3D printed components as dielectric materials, even if only in high-voltage devices, it is necessary to investigate both the relative permittivity  $\varepsilon_r$  of such products and their electric strength  $E_{bd}$ . The relative permittivity as a factor determining material's ability to store electrical energy in the electric field compared to a vacuum is necessary, among others, to adequately model the substrate for systems operating at higher frequencies, such as the manufacture of prototype antennas. The authors of the article [9] have shown that an antenna fabricated using this method meets the design assumptions and its parameters do not differ from commercial fabrications. The fabrication of analogue circuits operating at lower frequencies, from acoustic frequencies to tens of MHz, is associated with the need to know the relative permittivity of the substrate on which they are placed. When making multilayer PCBs, it is necessary to know the parasitic capacitances both between the paths carrying the various signals and between the components themselves. The authors of this paper ask whether the electrical properties of printed dielectric materials correspond to those of injection molding or casting, which are quite well known. In publication [10], the authors investigate the relative permittivity of dielectric materials used in printing in the frequency range from 100 µHz to 5 kHz, while in publication [11] the authors investigate in the range from 100 Hz to 1 kHz and in [8] from 0.01 Hz to 10 kHz.

This paper presents the study of the relative permittivity of FDM printed dielectrics in the acoustic frequency band from 20 Hz to 20 kHz using the three-electrode method and measuring with an LCR meter using a 4-wire setup. Such a setup is suitable for measurements in the frequency range up to 100 kHz [12, 13]. Analysis of the dielectric response in a wide frequency range is also used to determine the condition of transformer insulation [14].

Electric strength (alternatively called often as dielectric strength) can be expressed as the ratio of the voltage  $V_{bd}$  applied between the electrodes of a plate capacitor at the moment of dielectric breakdown of the material placed between these electrodes to specimen thickness w. It is an important parameter not only for use of 3D printing in PCB production, but also for high voltage applications such as housings or baffles, for example in voltage duplicators for X-ray heads.

Publications [9, 11, 15, 16], present research results with use of 50 Hz AC voltage excitation. In the paper [15], the breakdown strength of printed samples made of PLA, ABS, ASA, PETG, PC/ABS materials was tested. The effect of the shape of the specimens (cylindrical and square) on the breakdown voltage value was investigated. A statistical analysis of the results was carried out. The authors of this paper also lean towards this problem, as the use of this type of power supply is very common, but nevertheless consider it indispensable to also take into account the effects of voltage surges. This article presents the electric strength study carried out on 3D printed samples against lightning voltage surges using the Marx generator system [17]. In the view of the authors of this article, the effect of lightning surges on the electric strength of dielectric printed materials has not been sufficiently investigated. The performed research will help to understand, to some extent, whether it is appropriate to use the same assumptions for estimating parameters related to electrical breakdown electrical breakdown of materials obtained by 3D printing as for those made by injection molding or casting.

# 2. Materials, specimens and printing parameters

The most popular 3D model prototyping materials used by both professionals and amateurs were selected for the study. A series of samples were made of materials such as PLA (polylactide), ABS (acrylonitride-butadiene-styrene), PETG (polyethylene terephthalate glycol-modified), ASA (acrylonitrile styrene acrylate) and PETG FR (polyethylene terephthalate glycol-modified fire retardant), which is characterized by the addition of flame retardants. In order to eliminate the influence of dyes, all the filaments with diameter equal to 1.75 mm were chosen in black.

All specimens of each material were printed using the Fused Deposition Modeling (FDM) method with the printing parameters recommended by the manufacturer of each filament on a calibrated printer. In addition, one batch more of PLA material was printed on another uncalibrated printer (which is marked as PLA-2) to illustrate the effect of the printer itself and the accuracy of the printing on the measurement results. A large statistical sample was used for the study. For each material, 20 samples were produced. Figure 1(a) shows a prepared sample of PLA material.

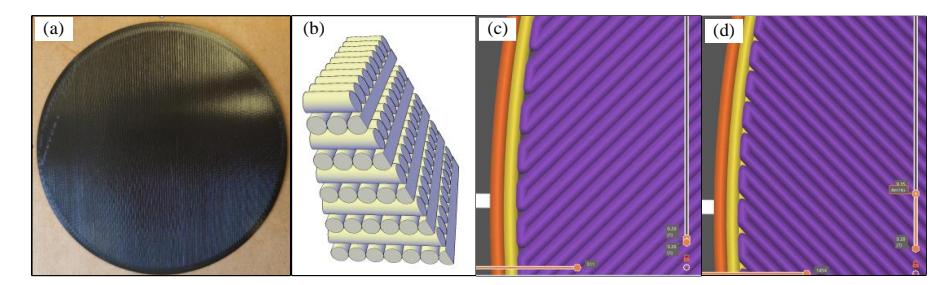


Fig. 1. View of prepared PLA sample (a); CAD model section of a sample (b); visualizations of the filament arrangement in the sample layer during the various stages of fabrication (c, d)

According to the authors, this number of samples represents a good compromise between obtaining satisfactory measurement uncertainty (for more details see Chapter 4) and the cost and time of printing the test samples. A summary of all the materials used in the study, together with the printing parameters, is shown in Table 1.

Parameter	PLA	PLA-2	ABS	PETG	ASA	PETG FR
Extruder temperature, °C	215	215	260	230	260	230
Bed temperature, °C	60	60	105	85	105	85
Layer thickness, mm	0.1	0.1	0.1	0.1	0.1	0.1
Infill, %	100	100	100	100	100	100
Printing speed, mm/s	150	150	150	150	150	150

Table 1. Materials used in the tests, along with the printing parameters

The dimensions of the specimens were adequate for correct measurements of both relative permittivity by noninvasive tests and electric strength based on destructive test results. IEC 60243-1 standard [18] specifies the dimensions of injection-molded thermoplastic samples as  $60 \times 60 \times 1$  mm. It also specifies diameter of at least 100 mm and a thickness of 1 mm for compression-molded samples. For the purposes of the research described in this paper, it was decided to fabricate disc-shaped samples with a thickness w of 1 mm and a diameter  $d_s$  of 85 mm. This provided both the optimal diameter for measuring relative permittivity (limiting the test stand to  $90 \times 90$  mm) and ensured the minimum dimensions required by the IEC standard for electric strength testing. The specimens were obtained from 10 layers of filament, each 0.1 mm thick (see Fig. 1(b)). Figures 1(c) and 1(d) shows a visualization of the arrangement of the filament in the sample layers during the various stages of printing.

Before relative permittivity measurements were performed, the samples were conditioned according to IEC 62631-2-1 [19]. Similarly, the same samples were then conditioned according to IEC 60243-1 [18] when it comes to electric strength.

# 3. Measuring setup

#### 3.1. Relative permittivity

Relative permittivity measurements were made indirectly by means of capacitance measurements with an LCR meter. The meter used was the GW INSTEK LCR-8110G (its basic accuracy of measurement was 0.1% of capacitance value), and parallel plate test fixture (see Fig. 2), made in accordance with the recommendations of IEC 62631-2-1 [19]. The measuring attachment was a classic three-electrode system with a guarding ring electrode. The electrodes of the test fixture were made of stainless steel ground to an accuracy of 0.02 mm, the housing was made of aluminum and milled to an accuracy of 0.1 mm, while the insulators were made of teflon with an accuracy of 0.1 mm. The upper movable high voltage electrode was equipped with a spring system that allowed it to be pressed down evenly in the case of uneven surfaces of the test sample. The top electrode outer diameter  $d_4$  was equal to guard ring electrode outer diameter  $d_3$  of 80 mm. The measuring electrode had outer diameter  $d_1$  of 60 mm and the gap between it and the guard ring (due to the high accuracy of the components) was only 0.5 mm. The fixture and LCR were connected in a four-wire circuit to ensure adequate compensation of parasitic capacitances of the

entire circuit (see Fig. 2). The meter used had the ability to automatically measure and average the results. For each specimen, capacitance measurements were made in the range from 20 Hz to 20 kHz with increments of 200 Hz. For each frequency, the measurement was performed 10 times and its value averaged by the meter, with the final results exported via RS-232 interface to a PC for further processing.

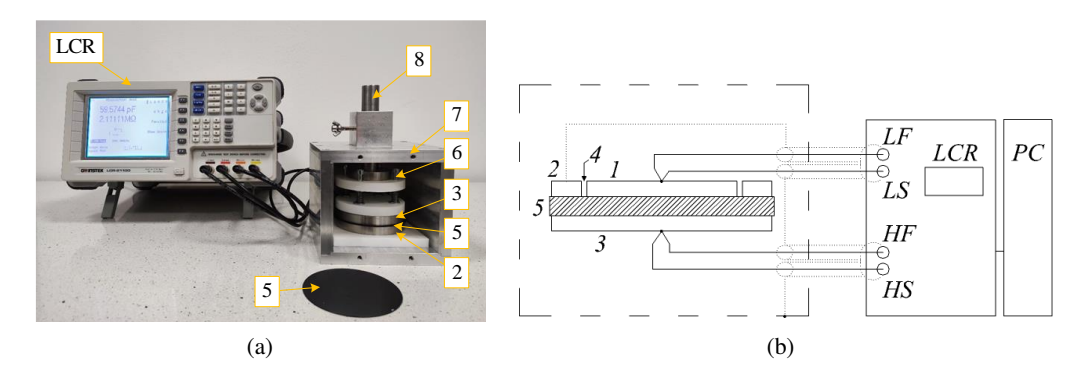


Fig. 2. The general view of the test stand (a); the scheme of measuring setup (b): "LCR" – LCR meter, 1 – measuring electrode, 2 – guard ring electrode, 3 – supply high voltage electrode, 4 – air gap, 5 – specimen, 6 – spring system, 7 – enclosure, 8 – pressure adjustment, "LF", "LS", "HF", "HS" – BNC ports of the meter, "PC" – computer. The dotted line indicates the shielding of the cables and the measuring cell

The relative permittivity was determined by (1) [13, 19]:

$$\varepsilon_r = \frac{C \cdot w}{\varepsilon_0 \cdot s},\tag{1}$$

where: C (pF) denotes the measured value of the capacitance, w (mm) is the thickness of the sample,  $\varepsilon_0 = 8.85 \cdot 10^{-3}$  (pF/mm) is the permittivity of vacuum and s (mm<sup>2</sup>) is the active surface of electrodes calculated using (2)

$$s = \frac{\pi}{4} \cdot (d_1 + B \cdot g)^2, \qquad (2)$$

where:  $d_1$  (mm) denotes the measuring electrode diameter, B (–) is the correction factor of the active surface of the electrodes and g (mm) is the width of the air gap between the protective and measuring electrodes. The correction factor was calculated using (3).

$$B = 1 - \frac{4 \cdot w}{\pi \cdot g} \cdot \ln \cosh \left( \frac{\pi \cdot g}{4 \cdot w} \right). \tag{3}$$

## 3.2. Electric strength at AC voltage

A setup complying with IEC 60243-1 [18] was used to measure the electric strength at AC voltage. A TP110 high voltage transformer with a 15-minute power of 10 kVA was used, which guaranteed a short-circuit current higher than that required by IEC standard. The transformer was connected to the measuring electrode system through a water resistor with a resistance of  $100 \text{ k}\Omega$ .

526 S. Hajder et al. Arch. Elect. Eng.

A Vitrek4700 meter with a 150 kV probe connected to the high-voltage electrode was used to measure the voltage (basic accuracy of measurement was 0.5%+10 V). The meter communicated with a PC via an Ethernet network. This meter provided a remote reading with an interval of 100 ms, which gave 5 values averaged over 5 periods of the measured voltage, allowing for a fairly accurate reading of the last voltage value before the breakdown of tested sample. In addition, low-voltage side readings were also recorded using a LUMEL digital meter, which averages values from 2 periods of measured voltage and has an option to store the last result. This was only a control measurement, since measurement through the transformer gear by using a  $100 \text{ k}\Omega$  damping resistor in series with the measuring electrode array is subject to greater uncertainty than direct measurement with Vitrek4700 with a divider on the high-voltage side. The entire test system had an adjustable and controllable test voltage rise rate through a remotely controlled auto-transformer, which value was set at 2 kV/s during the measurements. The test electrodes were 25 mm in diameter, made of stainless steel and ground on the face. The ambient medium for the measurements performed was dried transformer oil. Figure 3(a) shows the view of the measuring system, while Fig. 3(b) presents its schematic diagram.

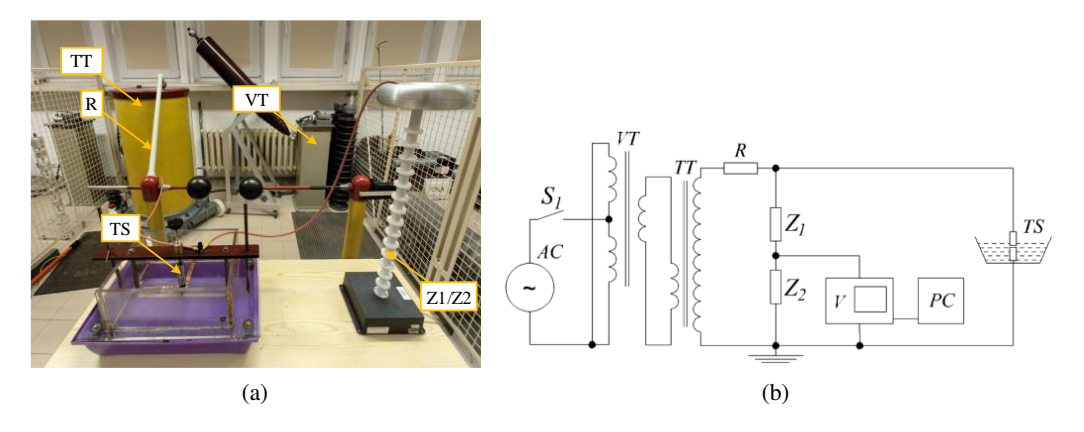


Fig. 3. The view of measuring system (a); the schematic diagram of setup (b): AC – power source, PC – computer, R – water resistor, S1 – switch, TS – test stand, TT – high voltage transformer, V – voltage divider control box, VT – voltage regulation transformer, Z1/Z2 – voltage divider

For both AC and surge voltage excitation, the electric strength  $E_{bd}$  (kV/mm) was determined as the quotient of the measured breakdown voltage  $V_{bd}$  (kV) and the thickness w (mm) of the sample:

$$E_{bd} = \frac{V_{bd}}{w}. (4)$$

#### 3.3. Electric strength at surge voltage

A setup according to the recommendations of part three of IEC 60243 [20] was used to measure the electric strength at lightning surge voltage (see Fig. 4). The tests were carried out using a three-stage Marx generator with a surge shaping system. A normalized 1.2/50 µs lightning voltage surge was obtained at the generator output. A measuring spark gap according to DIN EN 60052:2003 [21] was used to measure the voltage at the generator output with. The measuring

electrodes had a diameter of 25 mm, and were made of stainless steel. The ambient medium for the samples during the measurements was dried transformer oil. In contrast to AC tests, where a constant increase in voltage at the constant rate of rise value was used, in this case the tests were started at 70% of the expected breakdown voltage  $V_{bd}$  (based on AC measurements for the same material types) in a series of 10 identical pulses, and then if no breakdown has occurred the test voltage was increased.

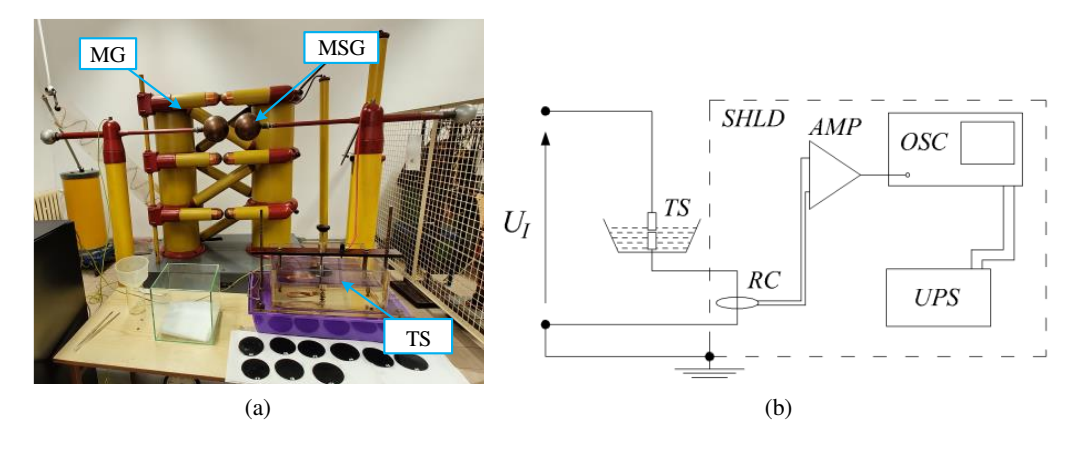


Fig. 4. The electric strength measurement setup for surge voltages (a); specimen breakdown detection circuit diagram (b): AMP – amplifier,  $U_I$  – surge voltage, MG – 3-stage Marx generator, MSG – measuring spark gap, OSC – oscilloscope, RC – Rogowski coil, SHLD – shield around the breakdown detection circuit, TS – test stand, UPS – uninterruptible power supply

Due to recommendations on the procedure for lightning surge voltage measurements in the standards, the following algorithm was used:

- 1. setting the distance on the measuring spark gap (resolution of 1 mm) corresponding to the desired peak voltage according to IEC standard table,
- 2. making a correction taking account of the atmospheric conditions in the laboratory room during the tests,
- 3. setting the so-called 50% disruptive discharge voltage  $U_{50}$  by adjusting the Marx generator,
- 4. testing the specimen with the pre-defined  $U_{50}$  voltage, and if no breakdown occurred with 10 impulses, the voltage was increased further.

Setting  $U_{50}$  voltage was performed for a test equal to 50 generator impulses – and the acceptable number of breakdowns on the measuring spark gap was  $25 \pm 1$ . According to the specification [21], the relative expanded uncertainty of the  $U_{50}$  peak voltage value at a confidence level of 95% was less than 3%. Unfortunately, IEC 60243-3 standard [20] does not describe the exact form of detection of breakdown during tests. The authors of the study proposed a monitoring system with the use of a Rogowski coil (Fig. 5(b)) attached to the return conductor from the test stand to the generator that was connected to the ground. The probe was connected to oscilloscope (OSC) powered with an uninterruptable power supply (UPS) placed in a shielded and earthed enclosure (SHLD) to eliminate possible interference. If a current waveform with significant amplitude was recorded in the return wire, the sample was considered to have been destroyed by electrical breakdown.

#### 4. Results

#### 4.1. Relative permittivity

The value of the relative permittivity  $\varepsilon_r$  was estimated mainly from measurements of the electrical capacitance C and thickness w for each of the 20 samples of the material. The values of the other quantities related to the dimensions of the measuring system used in Eq. (1–3) were practically comparable for each sample. The result for each capacitance measurement point, as already mentioned in the previous paragraph, was automatically averaged by the meter from 10 subsequent readings. The capacitance values for different samples within the same material at the same frequency diverged. In some cases, there are clearly extreme values that should be discarded in the measurements and treated as coarse error. The capacitance measurement data obtained, with a size of 20 samples, is subject to a Student's t-distribution with a number of degrees of freedom equal to 19 similar to a Gaussian normal distribution. Table 2 summarizes the results of calculating the mean value and relative standard deviation (RSD) of capacitance for selected frequencies of 20 Hz, 1 kHz, 10 kHz and 20 kHz.

Frequency	20 Hz		1 kHz		10 kHz		20 kHz	
Material	Mean [pF]	RSD [%]	Mean [pF]	RSD [%]	Mean [pF]	RSD [%]	Mean [pF]	RSD [%]
ABS	57.99	5.25	57.17	5.19	56.63	5.16	56.55	5.16
ASA	63.65	5.28	61.21	5.13	60.52	5.09	60.38	5.10
PETG	66.71	5.15	66.34	5.11	65.60	5.07	65.33	5.06
PETG FR	61.91	5.80	61.57	5.73	61.00	5.63	60.87	5.60
PLA	59.63	3.76	59.13	3.67	58.62	3.61	58.54	3.62
PLA-2	54.69	6.89	54.29	6.79	53.86	6.68	54.07	6.48

Table 2. Capacitance measurement results for selected frequencies

In accordance with the IEC 62631 [19] standard, relative permittivity was calculated from the average of the capacitance measurements for each frequency on the basis of Eqs. (1–3). The results of these calculations are shown in Fig. 5. Table 3 shows the results of the relative permittivity mean value and uncertainty of its estimation for the tested materials at 20 Hz.

An estimation of the relative permittivity measurement uncertainty was carried out. Its value was influenced mainly by the spread of the capacitance results. The determined uncertainty for the same material varied slightly with the frequency at which the measurement was performed, as can be seen in the case of capacitance (Table 2). As the uncertainty was calculated the same for different materials and frequencies, the detailed calculation of uncertainty was presented below only for PLA-2 material and the frequency of 20 Hz as an example. For this case the highest relative value of uncertainty was obtained and can be considered as the limit value for all measurements.

The procedure for the determination of the uncertainty included type A and B uncertainties depending on the result spread and the limiting errors of the measuring instruments. The combined

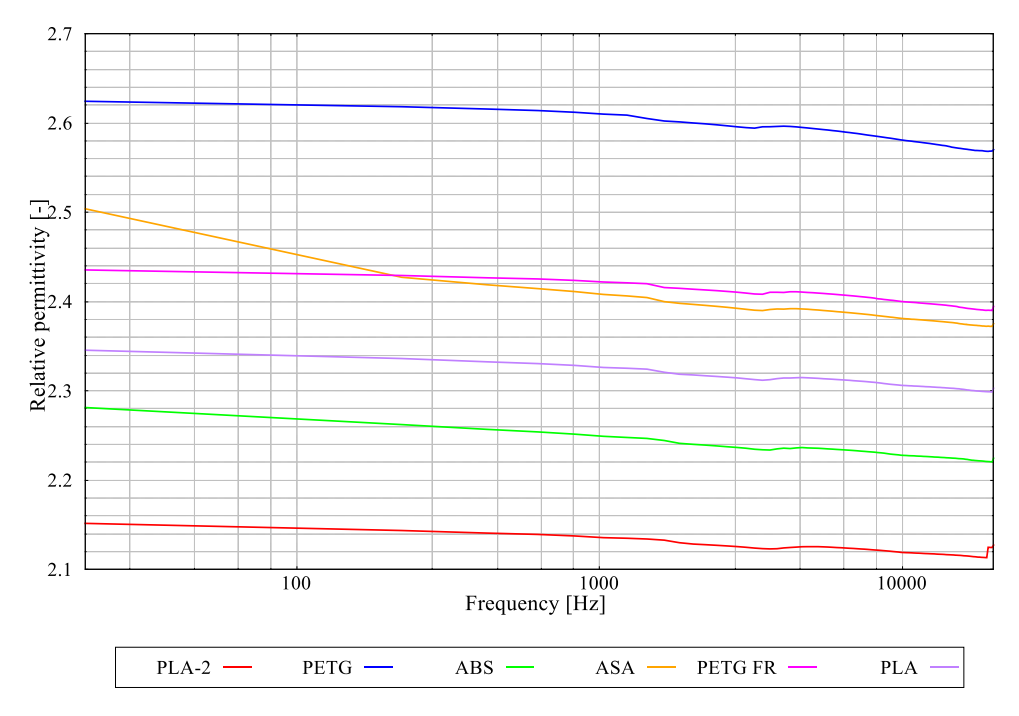


Fig. 5. Relative permittivity in function of frequency for every tested material

Table 3. The relative permittivity mean value and uncertainty of its estimation for all materials at  $20\ Hz$ 

Material	Mean value	Combined standard uncertainty	Coverage factor	Expanded uncertainty	Relative expanded uncertainty
	$\overline{\varepsilon}_r$ [–]	$u\left(\varepsilon_{r}\right)\left[-\right]$	k <sub>p</sub> [–]	$U\left( oldsymbol{arepsilon}_{oldsymbol{r}} ight) \left[ - ight]$	$U_{\mathrm{rel}}\left( arepsilon_{r} ight) \left[\% ight]$
ABS	2.282	0.059	2.23	0.131	5.74
ASA	2.504	0.065	2.23	0.144	5.75
PETG	2.625	0.067	2.23	0.150	5.72
PETG FR	2.436	0.064	2.20	0.141	5.79
PLA	2.346	0.057	2.31	0.132	5.64
PLA-2	2.152	0.059	2.16	0.128	5.97

uncertainty was calculated, the sensitivity coefficients and degrees of freedom were determined (Tables 4–6). Finally, the expanded uncertainty of relative permittivity mean value estimation (p = 95%) and its relative value were derived (see Table 3).

Table 4. Summary of uncertainty of relative permittivity  $\varepsilon_r$  estimation for PLA-2

Measured quantity $X_j$	Mean value $\overline{X}_j$	Sensitivity coefficient $c_j$	Standard uncertainty $u\left(X_{j}\right)$	$c_j^2 u^2 \left(X_j\right)$	Degrees of freedom $v_j$	
Capacitance C	54.69 pF	$39.34 \cdot 10^{-3}$ (pF) <sup>-1</sup>	0.84 pF	$1.1 \cdot 10^{-3}$	19	
Thickness w	0.999 mm	$2.153 \text{ (mm)}^{-1}$	0.023 mm	$2.4 \cdot 10^{-3}$	7	
Active surface s	2868.7 mm <sup>2</sup>	$-0.7501 \cdot 10^{-3}$ (mm) <sup>-2</sup>	1.9 mm <sup>2</sup>	$2.066 \cdot 10^{-6}$	40	
Relative permittivity $\varepsilon_r$	2.152	$\sum c_j^2 u^2 \left( X_j \right) =$	= 3.533 · 10 <sup>-3</sup>	13		
Combined standard uncertainty of relative permittivity estimation $u(\varepsilon_r) = 0.059$						

Table 5. Summary of combined standard uncertainty of active surface s calculation for PLA-2

Measured quantity $X_j$	Mean value $\overline{X}_j$	Sensitivity coefficient $c_j$	Standard uncertainty $u\left(X_{j}\right)$	$c_j^2 u^2 \left(X_j\right)$	Degrees of freedom $v_j$
Electrode diameter $d_1$	60.023 mm	94.934 mm	0.013 mm	1.494 mm <sup>4</sup>	7
Air gap width g	0.515 mm	76.225 mm	0.019 mm	2.023 mm <sup>4</sup>	364
Correction factor B	0.8029	48.891 mm <sup>2</sup>	$8.01 \cdot 10^{-3}$	0.1535 mm <sup>4</sup>	76
Active surface s	2868.7 mm <sup>2</sup>	= 3.671 mm <sup>4</sup>	40		
Combined standa	ard uncertainty	(s) = 1	.9 mm <sup>2</sup>		

Table 6. Summary of combined standard uncertainty of correction factor B calculation for PLA-2

Measured quantity $X_j$	Mean value $\overline{X}_j$	Sensitivity coefficient $c_j$	Standard uncertainty $u\left(X_j\right)$	$c_j^2 u^2 \left( X_j \right)$	Degrees of freedom $v_j$
Thickness w	0.999 mm	$0.18704 \; \mathrm{mm}^{-1}$	0.023 mm	$1.8341 \cdot 10^{-5}$	7
Air gap width g	0.515 mm	-0.36295 mm <sup>-1</sup>	0.019 mm	$4.5876 \cdot 10^{-5}$	364
Correction factor B	8.029	$6.4218 \cdot 10^{-5}$	76		
Combined standa	$.01 \cdot 10^{-3}$				

## 4.2. Electric strength

The electric strength  $E_{bd}$  measurements for both AC voltage and lightning surge voltage were performed for 10 samples of a given material. According to the IEC 60243-1 [18], the development of measurement results should be reduced to calculating the median breakdown voltage for a given material, but the authors decided to present results by determining arithmetic mean value and uncertainties, which characterize both the statistical data of the measurements and the accuracy of the measuring instruments. A summary of results for both AC and surge voltage is presented in Table 7.

Table 7. The comparison of electric strength mean value and uncertainty of its estimation for all materials at AC and surge voltage

Ma	aterial	Median value	Mean value	Combined standard uncertainty	Coverage factor	Expanded uncertainty	Relative expanded uncertainty
		[kV/mm]	$\overline{E}_{bd}$ [kV]	<i>u</i> ( <i>E<sub>bd</sub></i> ) [kV]	k <sub>p</sub> [kV]	$U(E_{bd})$ [kV]	$U_{\mathrm{rel}}\left(E_{bd} ight)$ [%]
	ABS	34.5	38.04	2.83	2.23	6.32	16.6
AC	ASA	28.8	28.69	2.43	2.23	5.42	18.9
voltage	PETG	21.7	23.60	2.52	2.26	5.70	24.1
	PETG FR	40.6	40.99	1.83	2.14	3.92	9.6
	PLA	29.0	28.69	1.31	2.14	2.81	9.8
	PLA-2	24.6	22.78	1.78	2.23	3.97	17.4
	ABS	45.4	45.14	2.84	2.12	6.01	13.3
surge	ASA	44.1	44.62	2.61	2.10	5.49	12.3
voltage	PETG	48.0	46.19	2.38	2.06	4.91	10.6
	PETG FR	61.7	61.15	1.96	2.06	4.04	6.6
	PLA	38.7	38.13	1.97	2.06	4.06	10.7
	PLA-2	37.3	37.29	2.03	2.09	4.26	11.4

Tables 8 and 9 show summaries of measurement uncertainty estimations for the PETG material tested at AC voltage.

Tables 10 and 11 show part of the uncertainty analysis of the electric strength measurement using the example of ABS material, for which the relative uncertainty takes on the highest value of all results.

532 S. Hajder et al. Arch. Elect. Eng.

Table 8. Summary of electric strength  $\mathcal{E}_{bd}$  uncertainty estimation for PETG and AC voltage

Measured quantity $X_j$	Mean value $\overline{X}_j$	Sensitivity coefficient $c_j$	Standard uncertainty $u\left(X_{j}\right)$	$c_{j}^{2}u^{2}\left( X_{j} ight)$	Degrees of freedom $v_j$
Breakdown voltage $V_{bd}$	23.59 kV	1.0006 mm <sup>-1</sup>	2.46 kV	6.06 (kV/mm) <sup>2</sup>	9
Thickness w	0.999 mm	- 23.62 kV (mm) <sup>-2</sup>	0.023 mm	0.29 (kV/mm) <sup>2</sup>	7
Electric strength $E_{bd}$	23.60 kV/mm	_	$\sum c_j^2 u^2 (X_j)$	$\sum c_j^2 u^2 \left( X_j \right) = 6.3499$	
Combined standa	.52 kV/mm				

Table 9. Summary of breakdown voltage  $V_{bd}$  measurement uncertainty for PETG and AC voltage

Quantity $X_j$	Standard uncertainty $u\left(X_j\right)$	Degrees of freedom $v_j$	Comment
$u_{A}\left( V_{bd}\right)$	2.46 kV	9	Type A standard uncertainty of mean value estimation of 10 measurements
$u_{B1}\left(V_{bd}\right)$	0.07 kV	∞	Type B standard uncertainty of measurement with a Vitrek 4700 voltmeter (accuracy = $0.5\% + 10 \text{ V}$ )
$u_{B2}\left(V_{bd}\right)$	0.17 kV	ω	Type B standard uncertainty depended on both the voltage rise rate of 2 V/ms and voltmeter RMS value calculation time of 100 ms
$u(V_{bd})$	2.46 kV	76	$u\left(V_{bd}\right) = \sum u^2\left(X_j\right)$

Table 10. Summary of electric strength  $E_{bd}$  uncertainty estimation for ABS and surge voltage

Measured quantity $X_j$	Mean value $\overline{X}_j$	Sensitivity coefficient $c_j$	Standard uncertainty $u\left(X_{j}\right)$	$c_{j}^{2}u^{2}\left( X_{j} ight)$	Degrees of freedom $v_j$	
Breakdown voltage $V_{bd}$	45.11 kV	1.0006 mm <sup>-1</sup>	2.64 kV	6.97 (kV/mm) <sup>2</sup>	13	
Thickness w	0.999 mm	- 45.16 kV (mm) <sup>-2</sup>	0.023 mm	1.07 (kV/mm) <sup>2</sup>	7	
Electric strength $E_{bd}$	45.14 kV/mm	-	$\sum c_j^2 u^2 (X_j) = 8.041 \text{ (kV/mm)}^2$		16	
Combined standard uncertainty of electric strength estimation $u(E_{bd}) = 2.8$						

Standard Quantity Degrees of uncertainty Comment  $X_j$ freedom  $v_i$  $u(X_i)$ Type A standard uncertainty of mean value estimation 2.39 kV 9  $u_A(V_{bd})$ of 10 measurements. Type B standard uncertainty resulting from the evaluation of the result based on the reading of the IEC table  $u_{B1}\left(V_{bd}\right)$ 0.78 kV  $\infty$ and the consideration of weather conditions correction factor (less than 3%). Type B standard uncertainty due to an error in the reading of the dial indicator of the HV measuring  $u_{B2}(V_{bd})$ 0.79 kV electrode spacing (of approximately 0.5 mm) as well  $\infty$ as in the interpolation of the tabulated data (average variation of 2.75 kV/mm). 2.64 kV 13  $u\left(V_{bd}\right) = \sum u^2 \left(X_j\right)$  $u\left(V_{bd}\right)$ 

Table 11. Summary of breakdown voltage  $V_{bd}$  measurement uncertainty for ABS and surge voltage

Failure probability analysis based on the cumulative distribution function (CDF) of the Weibull distribution (5) is a popular method used in reliability analysis and equipment life prediction:

$$F(x) = f(x) = \begin{cases} 0, & x < 0 \\ 1 - e^{-(x/\lambda)^k}, & x \ge 0 \end{cases}$$
 (5)

where: x is a random variable (e.g. time to failure),  $\lambda > 0$  is the scale parameter and k > 0 is the shape parameter. For both AC and surge test voltages, this procedure was performed for the electrical strength results obtained previously. As a result, the breakdown probability (6) was determined as a function of  $E_{bd}$  that corresponds to the theoretical Weibull function (5):

$$p_{bd}(E_{bd}) = \begin{cases} 0\%, & E_{bd} < 0\\ \left(1 - e^{-(E_{bd}/\lambda)^k}\right) \cdot 100\%, & E_{bd} \ge 0 \end{cases}$$
 (6)

First, an experimental estimate of the distribution function was defined, where its value for each data point  $E_{bd}$  was calculated using (7):

$$p_{\text{exp\_est}}(E_{bd}, i) = \frac{i}{N+1} \cdot 100\%,$$
 (7)

where: i corresponds to the number of observations in the sorted record of  $E_{bd}$  electrical strength values and N is the number of all observations (here N=10). In a further step, a polynomial regression was performed using the least squares method and the parameters  $(\lambda, k)$  of the breakdown probability function  $p_{bd}$  ( $E_{bd}$ ) were determined. This one is valuable for comparing with each other the behaviour of tested materials depending on the electrical strength values, especially for the risk of electrical breakdown assessment. Plots of  $p_{bd}$  ( $E_{bd}$ ) functions (solid lines) against functions  $p_{\text{exp\_est}}$  ( $E_{bd}$ , i) (as markers) for both AC and lightning surge voltage tests are presented in Figs. 6 and 7, respectively. The graphs include computed values of  $\lambda$  and k (the shape and the scale) parameters calculated for each of the materials tested and also the  $R^2$  coefficient of determination.

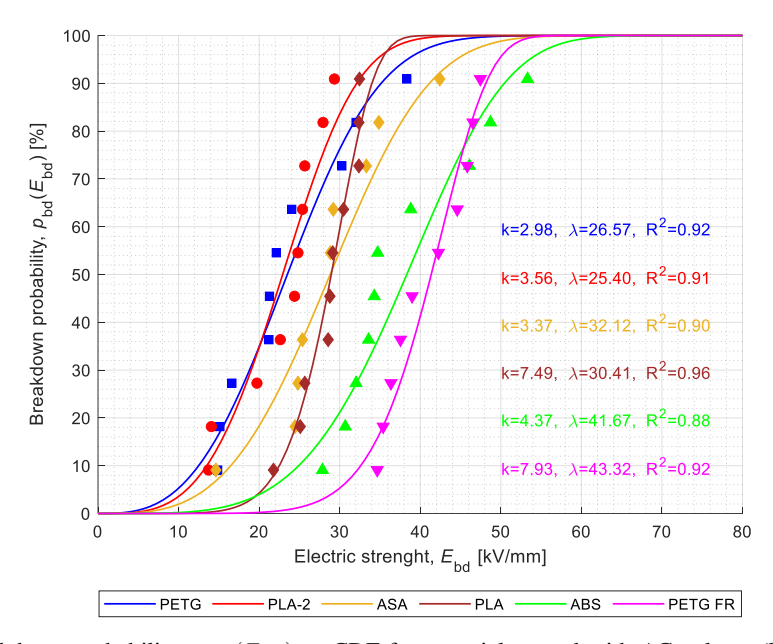


Fig. 6. Breakdown probability  $p_{bd}\left(E_{bd}\right)$  as CDF for materials tested with AC voltage (lines) against experimental distribution function  $p_{\text{exp\_est}}\left(E_{bd},i\right)$  (as markers)

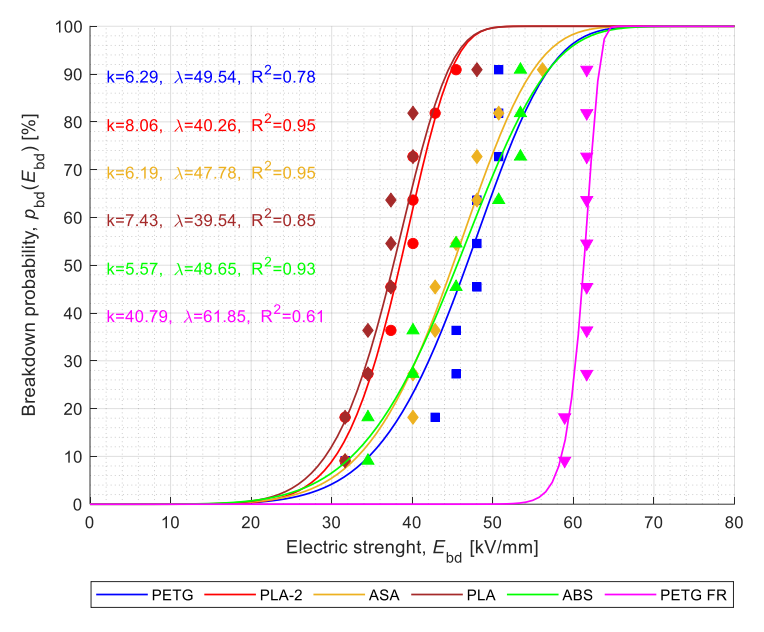


Fig. 7. Breakdown probability  $p_{bd}\left(E_{bd}\right)$  as CDF for materials tested with surge voltage (lines) against experimental distribution function  $p_{\text{exp\_est}}\left(E_{bd},i\right)$  (as markers)

## 5. Analysis and discussion

The relative permittivity tests have shown that, using of conventional methods of measuring capacitance in a three-electrode system, the obtained permittivity results for all tested materials had an expanded relative uncertainty in the range of 5.5%-6% (see Table 3). Despite the use of identical 3D printer settings and electrode system with the same pressure, for all samples some of them significantly differed from the average value in terms of the intended capacitance. In the authors' opinion, the accuracy of 3D printing influenced both the inhomogeneity of the internal structure of the samples and their thickness w. Both of these effects (resultant sample capacitance C and thickness w) influenced the estimated final relative permeability  $\varepsilon_r$  result, as can also be seen in the uncertainty analysis (sensitivity coefficients) shown in Tables 4–6.

Nevertheless, the capacitance readings were averaged and then the relative permittivity  $\varepsilon_r$  values were determined for each frequency point. The highest permittivity (2.57–2.63) is characteristic of PET-G, slightly lower (2.40–2.44) of PET-FR with flame retardant additives. The ASA material shows a significant decrease from 2.5 to 2.4 in relative permittivity in the range up to 200 Hz, above this frequency it behaves very similarly to the other materials. All materials show slight changes in relative permittivity in the tested frequency band, as can be seen in other studies, including publication [8]. The ABS material shows permittivity at a level of 2.24–2.28, and PLA at a level of 2.32–2.35. Comparing the results of ABS and PET-G measurements with the results presented in the article [11], it can be assumed that they are convergent. Differences appear when trying to compare the most commonly used in 3D printing – PLA material.

In this article, the authors tested samples printed on a calibrated printer and an uncalibrated one, which left uneven distribution of subsequent print lines and layers. The structures observed under digital microscope KEYENCE VHX-970F (CMOS sensor, 1/1.8 inch, 3.19 megapixel, with VH-Z100R wide-range (1001 to 10001) zoom lens) show the formation of air gaps between subsequent strips of melted material (see Fig. 8(a)), which is reflected in the relative permittivity measurements. The graph presented in Fig. 5 clearly shows that samples with worse, less accurate printing, marked PLA-2, are characterized by lower relative permittivity than samples without defects (PLA). The authors of the article [11] reach similar conclusions, who compare different printing resolutions. The greater the path of the printed material was, and thus the larger the air gaps, the lower the relative permeability was obtained.

The tests of electric strength  $E_{bd}$  at alternating current showed that the highest electric strength was characteristic of the PETG FR (40.99 kV/mm) and ABS (38.04 kV/mm) materials. Tables 7 to 9 contain the measurement results including the uncertainty. Large values for the relative measurement uncertainty of  $E_{bd}$  can be seen, for PETG it is as high as 24%. This situation was mainly influenced by the type A uncertainty in the measurement of the breakdown voltage  $V_{bd}$  (as shown in Table 9), thus mainly the influence of the phenomena responsible for the breakdown mechanism at AC voltage and the influence of the low samples number became visible. Analysing results in Table 7 and Fig. 6, it can be seen that all measurements are characterized by a large discrepancy. Perhaps increasing the statistical sample by a larger number of specimens would improve the resolution of the results, however, with 10 specimens, it can be stated that the PLA material has the greatest uniformity in terms of the Weibull plot. In addition, differences can be found between the electric strength of the PLA and PLA-2 materials, where air inclusions in the print certainly contributed to the lower electric strength of the PLA-2 samples. The authors

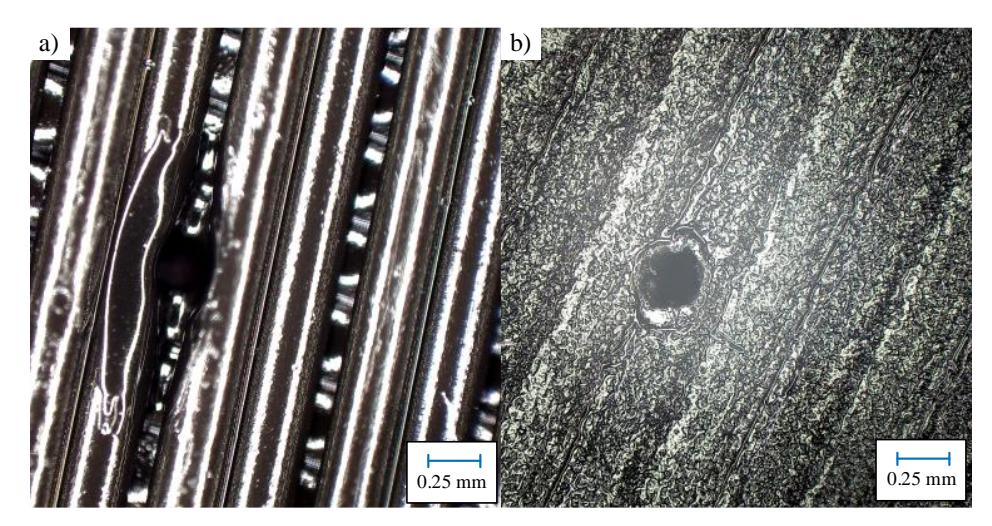


Fig. 8. Microscopic images of PLA-2 (a) and PET FR (b) samples with visible effects of calibration on print quality

of the article [6] reach a similar conclusion. Comparing the obtained results with those in the article [16], the values determined for PLA material appear to be similar. In the article [7], the values of breakdown voltages for PLA range from about 25 kV to 30.5 kV, whereas the test results presented in this paper are in the range of 22 kV and 32.5 kV, which corresponds to the results in article [11]. The analysis of the ABS material provides slightly different conclusions, namely the authors of this article obtained coverage from 28 kV to 54 kV, where in the article [16] it is 29 kV to 35 kV, respectively.

Comparing the summary of all electric strength  $E_{bd}$  measurement results at the AC excitation to publication [10], it can be concluded that for PLA and PET the results appear to be similar, while the results for ABS clearly differ. However, the authors in [10] performed measurements for sample thicknesses of 0.12 mm and 0.5 mm, followed by a so-called "thickness compensation", with such a comparison, the results seem to converge.

In the paper [15], slightly lower strength values were obtained for the individual materials. However, if the results of the respective materials are compared with each other, the conclusion is the same as for the results presented in this paper. The highest strength was recorded for ABS (30.28 kV/mm), PC/ABS (30.14 kV/mm), PETG (27.55 kV/mm), PLA (23.45 kV/mm) and ASA (20.35 kV/mm), respectively.

Electric strength measurements at surge voltages were characterized by an almost 10 times higher contribution of type B uncertainty of the surge voltage measurement to the final combined uncertainty compared to the tests at AC voltage (see Tables 9 and 11) mainly due to the measurement method using measuring spark gap. Despite this, the relative uncertainty of the  $E_{bd}$  measurement was 13.3% in the worst case (ABS). Test showed the lowest electric strength  $E_{bd}$  for PLA and PLA-2 materials. In the case of these tests, it did not matter whether the sample had air inclusions (PLA-2) or was printed on a correctly calibrated printer (PLA). ABS, ASA and PETG materials showed electric strength in the range of about 32 kV to 55 kV. Looking at the Weibull plot (Fig. 7), it can be assumed that their breakdown probability functions at surge voltage are very similar. On the other

hand, PETG FR with flame retardant additives was characterized by the highest strength. Authors believe that this high value of  $E_{bd}$  may be caused precisely by the use of additives to prevent rapid ignition of the material, perhaps these additives to some extent cause a reduction in electric field inhomogeneity at fast pulses, as in the case of the tests with lightning voltage surges. Unfortunately, these additives are a trade secret of the manufacturer, and tests with different percentages of these admixtures could not be carried out. The authors have not encountered published work on investigating the effects of lightning surge voltage on 3D printed specimens, hence they could not refer to such studies. Microscopic observation of puncture-damaged samples also yields interesting conclusions. It does not matter whether AC or lightning strike tests, the puncture practically always occurred between successive layers of printed material as was shown in Fig. 9.

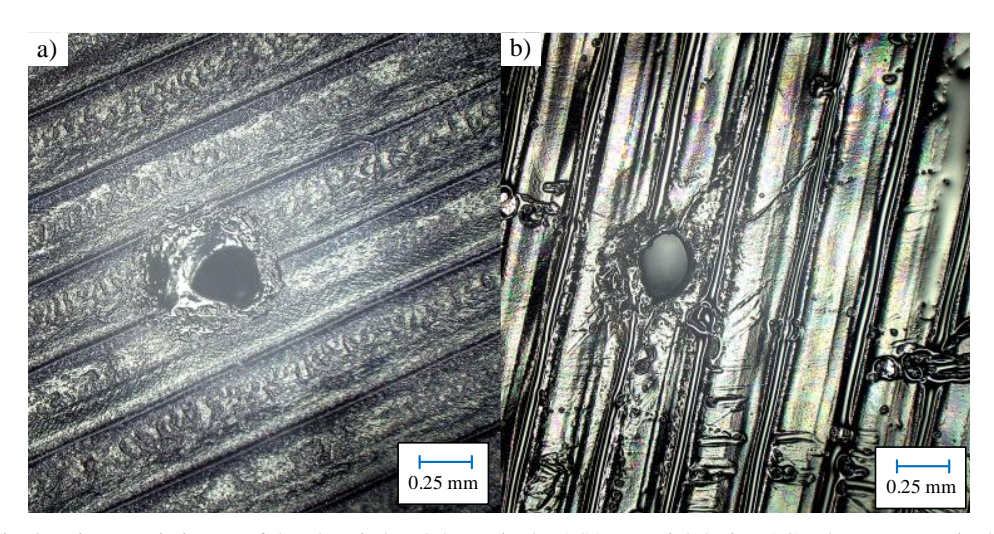


Fig. 9. Microscopic image of the electric breakdown: in the ASA material during AC voltage test (a); in the PET material during surge voltage test (b)

# 6. Conclusions

The study of the relative permittivity  $\varepsilon_r$  and electric strength  $E_{bd}$  of specimens made from different materials using the 3D printing technique was presented. Based on the experiments carried out and their results, the most important conclusions of practical relevance are formulated below.

The precision and quality of the 3D printing affects the relative permittivity of the material. PLA samples produced with an uncalibrated printer (marked as PLA-2) had lower values of  $\varepsilon_r$  compared to samples of the same material made with a calibrated printer (labelled as PLA), mainly due to the presence of air inclusions between the layers of the filament visible under the microscope. No apparent effect of these imperfections present in the PLA-2 material on the change in the expected (decreasing) frequency dependence of permeability was observed.

The determination and drawing the cumulative distribution function (CDF) of the Weibull distribution was a useful way of comparing with each other the behaviour of tested materials in relation to electrical strength values, particularly for assessing the risk of electrical breakdown.

The result of comparing the electric strength of materials when tested with surge voltage is completely different than with AC voltage. Therefore, conclusions drawn based on AC voltage tests should not be generalized to the case of exposing materials to lightning impulse voltage. The authors have not yet encountered any published studies on 3D-printed materials using this type of pulses. The demonstrated differences with respect to tests for AC voltages state that research in this direction should be continued. PLA and PLA-2 (with lower printing precision) materials exhibited nearly identical behaviour under voltage surges. However, for AC voltage, PLA-2 had lower dielectric breakdown strength.

The material with the highest dielectric breakdown strength under both AC voltage and lightning impulse voltage was found to be PETG FR. The high  $E_{bd}$  value may result from flame-retardant additives that prevent rapid ignition, potentially reducing electric field inhomogeneity during fast pulses, as seen with lightning surges. However, the composition of the additives is proprietary to the manufacturer, making it impossible to carry out comparative tests with different admixture contents.

In the printing technique used in the studies described in this article, where, from a top-down view, the filament alignment in every other layer remained consistent without an offset smaller than the filament thickness, "weak points" are formed at the intersections of print line boundaries between successive layers. As observed in microscopic images, these points are potential discharge initiation places, leading to dielectric breakdown under both AC and surge voltages. Therefore, to improve breakdown resistance, introducing a print line offset should be considered.

Based on the presented balance of measurement uncertainty for both permittivity and electric strength, it was noted that the total measurement uncertainty of their values is mainly influenced by type A uncertainty components, which depend, among other things, on the sample size. In most cases, the accuracy of the instruments and measurement methods only affected 5% of the total uncertainty obtained. The number of samples was, for economic and time reasons, limited to 10 for each material for measurements at high voltage. For sample sizes above 25, the results presented would have a narrower confidence interval.

#### References

- [1] Wimpenny D.I., Pandey P.M., Kumar L.J., *Advances in 3D Printing & Additive Manufacturing Technologies*, Singapore: Springer Singapore (2017), DOI: 10.1007/978-981-10-0812-2.
- [2] Cano-Vicent A. et al., Fused deposition modelling: Current status, methodology, applications and future prospects, Additive Manufacturing, vol. 47, 102378 (2021), DOI: 10.1016/j.addma.2021.102378.
- [3] Tan H.W., Choong Y.Y.C., Kuo C.N., Low H.Y., Chua C.K., 3D printed electronics: Processes, materials and future trends, Progress in Materials Science, vol. 127, 100945 (2022), DOI: 10.1016/j.pmatsci.2022.100945.
- [4] Macdonald E. et al., 3D Printing for the Rapid Prototyping of Structural Electronics, IEEE Access, vol. 2, pp. 234–242 (2014), DOI: 10.1109/ACCESS.2014.2311810.
- [5] Wałpuski B., Słoma M., *Accelerated Testing and Reliability of FDM-Based Structural Electronics*, Applied Sciences, vol. 12, 1110 (2022), DOI: 10.3390/app12031110.
- [6] Grant K., Zhang S., Kettle J., Improving the sustainability of printed circuit boards through additive printing, 2023 IEEE Conference on Technologies for Sustainability (SusTech), Portland, OR, USA, 2023, pp. 86–90 (2023), DOI: 10.1109/SusTech57309.2023.10129587.

- [7] Zdráhal J., Klimtová M., Králová I., 3D Printed Circuit Boards from Recycled Plastics: Interconnection Properties, 2024 47th International Spring Seminar on Electronics Technology (ISSE), Prague, Czech Republic, pp. 1–6 (2024), DOI: 10.1109/ISSE61612.2024.10603755.
- [8] Sekula R., Immonen K., Metsa-Kortelainen S., Kuniewski M., Zydroń P., Kalpio T., Characteristics of 3D Printed Biopolymers for Applications in High-Voltage Electrical Insulation, Polymers (Basel), vol. 15 (2023), DOI: 10.3390/polym15112518.
- [9] Huber E., Mirzaee M., Bjorgaard J., Hoyack M., Noghanian S., Chang I., *Dielectric property measurement of PLA*, 2016 IEEE International Conference on Electro Information Technology (EIT), Grand Forks, ND, USA, pp. 788–792 (2016), DOI: 10.1109/EIT.2016.7535340.
- [10] Schmid A., Modrow N., Humpert C., Breakdown strength and dielectric properties of stereolithography 3D-printed dielectrics for high voltage applications, 23rd International Symposium on High Voltage Engineering (ISH 2023), Berlin, Germany, pp. 1242–1248 (2023), DOI: 10.1049/icp.2024.0794.
- [11] Veselý P., Tichý T., Šefl O., Horynová E., Evaluation of dielectric properties of 3D printed objects based on printing resolution, 5th International Conference Recent Trends in Structural Materials, Pilsen, Czech Republic (2018), DOI: 10.1088/1757-899X/461/1/012091.
- [12] Basics of Measuring the Dielectric Properties of Materials, Application Note, https://www.keysight.com.
- [13] Lisowski M., Measurements of Electrical Resistivity and Permittivity of Solid Dielectrics, Publishing House of Wrocław University of Science and Technology (in Polish), Wrocław, 2004..
- [14] Bigdeli M., Aghajanloo J., Condition assessment of transformer insulation using dielectric frequency response analysis by artificial bee colony algorithm, Archives of Electrical Engineering, vol. 65, no. 1, pp. 45–57 (2016), DOI: 10.1515/aee-2016-0004.
- [15] Uydur C.C, Assessment of Dielectric Strength for 3D Printed Solid Materials in Terms of Insulation Coordination, Applied Sciences, vol. 14, 11860 (2024), DOI: 10.3390/app142411860.
- [16] Li X.-R., Guo J., Li W.-D., Zhang L.-Y., Wang C., Guo B.-H. et al., Analysis of Morphology and Electrical Insulation of 3D Printing Parts, 2018 IEEE International Conference on High Voltage Engineering and Application (ICHVE), Athens, Greece, pp. 1–4 (2018), DOI: 10.1109/ICHVE.2018.8642096.
- [17] Hajder S., *Identification and Mitigation of overvoltages During Marx Generator Operation in Circuits Supplying Measurement Systems*, Scientific Journals of Rzeszów University of Technology Series Electrotechnics (in Polish), vol. 28, pp. 33–49 (2022), DOI: 10.7862/re.2022.3.
- [18] IEC 60243-1:2013, Electric strength of insulating materials Test methods Part 1: Tests at power frequencies (2013).
- [19] IEC 62631-2-1:2018, Dielectric and resistive properties of solid insulating materials Part 2-1: Relative permittivity and dissipation factor – Technical Frequencies (0.1 Hz – 10 MHz) – AC Methods (2018).
- [20] IEC 60243-3:2013, Electric strength of insulating materials Test methods Part 3: Additional requirements for 1.2/50 µs impulse tests (2013).
- [21] Verband Deutscher Elektrotechniker, DIN EN 60052:2003, Voltage measurements by means of standard air gaps (2003).